17th International Conference on Environmental Science and Technology

Athens, Greece, 1 to 4 September 2021

# Silver decorated $TiO_2$/g-$C_3N_4$ nanocomposites for photocatalytic elimination of water pollutants under UV and artificial solar light

**Islam Ibrahim[a,b,c], George V. Belessiotis[a], Andreas Kaltzoglou[d], Fotios Katsaros[a], Tarek M. Salama[c], Polycarpos Falaras[a]**

**a** Institute of Nanoscience and Nanotechnology, National Centre for Scientific Research (NCSR) "Demokritos", 15341 Agia Paraskevi, Athens, Greece.

**b** Department of Chemistry, National and Kapodistrian University of Athens, Zografou 15784, Greece.

**c** Department of Chemistry, Faculty of Science, Al-Azhar University, Nasr City, Cairo, 11884, Egypt.

**d** Theoretical and Physical Chemistry Institute, National Hellenic Research Foundation, 48 Vassileos Constantinou Avenue, 11635, Athens, Greece.

*corresponding author: Polycarpos Falaras
e-mail: p.falaras@inn.demokritos.gr

## Abstract

$TiO_2$/g-$C_3N_4$/Ag nanocomposites were prepared and used as highly efficient photocatalysts. $TiO_2$ nanoparticles were first prepared using a sol-gel process, and titania herostructures with varying amounts of graphitic carbon nitride (g-$C_3N_4$) were created using a hydrothermal technique. Following impregnation in a silver nitrate aqueous solution employing sodium citrate, the $TiO_2$/g-$C_3N_4$ heterostructures were decorated with Ag nanoparticles. The prepared materials exhibit strong photocatalytic activity in both oxidation and reduction reactions. Under UV and artificial solar illumination, the degradation of four model contaminants, methylene blue (MB), rhodamine B (RhB), 4-nitrophenol (4-NP), and chromium(VI) ($Cr^{+6}$), was examined. With degradation percentages of up to 95% for MB and 89% for RhB, an optimal condition was determined, resulting in the effective removal of dye contaminants under UV light. Fast degradation rates for these dyes were also observed under artificial solar light. In addition, the $TiO_2$/g-$C_3N_4$/Ag nanocomposites were successful during photocatalytic reduction of 4-NP and $Cr^{+6}$ contaminants in water, converting these hazardous compounds to a useful industrial precursor (aminophenol) and a less toxic substance ($Cr^{+3}$), respectively.

**Keywords:** $TiO_2$/g-$C_3N_4$/Ag nanocomposites; UV and artificial solar light; Organic-inorganic pollutants degradation.

## 1. Introduction

Removing contaminants from our environment is becoming one of the most urgent issues in the world (Antoniadou, Arfanis, Ibrahim, & Falaras, 2019; Chen et al., 2019; Ibrahim, Belessiotis, et al., 2020). The presence of organic-inorganic contaminants in drinking water (especially nitroaromatic compounds, hexavalent chromium, and dyes), causes a variety of diseases involving the liver, kidneys, and nervous system (Ibrahim, Ali, Salama, Bahgat, & Mohamed, 2016). Various out-of-date techniques, such as incineration, stripping process, biological technique, and activated carbon adsorption method, have been used to remediate the harm of environmental pollution. On the other hand, these methods produce secondary emissions that are harmful to our environment. In the context of green chemistry, semiconductor photocatalytic technology offers numerous benefits such as high efficiency, low energy consumption, and effective wastewater treatment. Due to its low cost, non-toxicity, chemical stability, and high photocatalytic activity, titanium dioxide ($TiO_2$) is a major semiconductor that is widely used in environmental application technology (Alamelu & Ali, 2020). However, $TiO_2$ has two major drawbacks: a large band gap of 3.2 eV in the anatase form compared to a standard hydrogen electrode (SHE), which allows only UV light (approximately 5% of solar light) to excite it (Ibrahim, Kaltzoglou, et al., 2020), and instant electron-hole recombination, which limits its functional and photocatalytic applications (Asahi, Morikawa, Irie, & Ohwaki, 2014). As a result, various methods for enhancing photocatalytic operation have been proposed, including coupling with another semiconductor, loading noble metals, and constructing heterojunctions (Park et al., 2013). Graphitic carbon nitride (g-$C_3N_4$), a polymeric semiconductor material with a bandgap of 2.7 eV, has attracted the interest of researchers due to its fascinating properties (Masih, Ma, & Rohani, 2017). g-$C_3N_4$ is an excellent semiconductor for a variety of photocatalytic applications such as $H_2$ evolution, $CO_2$ photoreduction, wastewater treatment, and solar cell applications (Antoniadou et al., 2019). However, since photogenerated $h^+$ and $e^-$ recombine quickly, which results in poor

photocatalytic properties, combining the benefits of pristine g-$C_3N_4$ and $TiO_2$ could be a good way to enhance the photocatalytic redox pathway. Wang et al. (Jiang et al., 2018) synthesized heterostructured $TiO_2$/g-$C_3N_4$ catalysts for photocatalytic redox reactions in the presence of sunlight. Moreover, because of their ability to trap electrons, silver nanoparticles may reduce the number of defects in $TiO_2$ by reducing electron-hole recombination. Furthermore, silver nanoparticles have the tendency to increase visible light absorption due to a surface plasmonic resonance (SPR) effect (Wei, Yu, & Huang, 2020).

In this study, we construct a tertiary nanostructure material $TiO_2$/$CN_x$/Ag with different titania/carbon nitride ratios and investigate the photocatalytic redox reactions under UV and artificial solar light. The structural, morphological and optoelectronic properties of the nanocomposite heterostructures were thoroughly investigated MB, RhB, 4-NP, and $Cr^{+6}$ were chosen as model contaminants to evaluate the photocatalytic efficiency of the photocatalysts as a function of titania/carbon nitride ratio.

## 2. Experimental

### 2.1. Materials

All chemicals were of high purity and were used as received from the companies. Titanium (IV) n-butoxide (≥99%), potassium bromate, potassium iodide, benzoquinone, isopropyl alcohol, oxalic acid (≥98%), absolute ethanol (≥99%) were purchased from Acros-Organics. Glacial acetic acid (≥98%), trisodium citrate (≥98%), 1,5-Diphenylcarbazide (≥98%), silver nitrate (≥99%) and spin trap 5,5-dimethyl-1-pyrroline N-oxide (DMPO) were all purchased from Sigma-Aldrich. Melamine, hydrochloric acid (37%), potassium hydroxide and potassium chloride purchased from Chem-Lab.

### 2.2. Preparation of $TiO_2$ using sol-gel technique

The sol-gel technique was used to create $TiO_2$ nanopowder (Ye, Chen, Xu, Geng, & Cai, 2018). First, we prepared solution (A) by continuously stirring 30 mL titanium (IV) n-butoxide and 120 mL absolute ethanol. Second, a solution (B) was prepared by combining 30 mL absolute ethanol, 12 mL DI $H_2O$, and 6 mL glacial acetic acid with 0.1 mol $L^{-1}$ HCl to acidify the solution to pH around 2, followed by dropwise addition to solution (A) with vigorous stirring for 15 min. After 3 hours of settling, a yellow transparent gel was acquired. Finally, a thermal treatment was carried out, which included drying at 100 °C overnight, grinding, annealing at 300 °C for 1 hour, and then increasing the temperature to 450 °C for 2 hours with a ramp rate of 5 °C /min. In order to synthesize the g-$C_3N_4$-$TiO_2$ composite materials, the $TiO_2$ synthetic procedure was repeated by adding appropriate g-$C_3N_4$ quantities into the mixture of solutions (A) and (B), under intensive stirring for 30 minutes. It is noted that the solution volume was reduced to one third, without changing the precursors' concentration. The final mixture was transferred to a 300 ml autoclave and heated at 180 °C for 24 hours (Crake et al., 2019). Afterwards, the precipitate was collected, dried at 100 °C and grinded. Finally, a two-step thermal treatment was applied at 300 °C for 1 h and then 450 °C for 2 h (ramp rate 5 °C /min). The final products are denoted as TCx, where x is the added g-$C_3N_4$ quantity (in mg): 100, 200 and 300. The silver nanoparticles were introduced onto the TCx composites with a reduction chemical method. First, 0.157 g $AgNO_3$ were dissolved in 6 ml DI $H_2O$ and then 0.9 g of TCx were added and soaked for 3 hours. Next, a 30 ml sodium citrate solution (0.27 g) was added dropwise, as reducing agent, and the final solution was stirred at 80°C until dry. The denoted as TCx@Ag composite materials were washed several times with hot DI $H_2O$ and dried at 100 °C.

### 2.3. Photocatalytic oxidation/ reduction experiments

The photocatalytic activity of the photocatalysts was evaluated by the photocatalytic reduction of $Cr^{6+}$ (50 mg/L) and (4-NP) (20 mg/L), and the photocatalytic oxidation of the organic dyes, (MB) (20 mg/L) and (RhB) (10 mg/L). The photocatalysts were placed in 50 ml aqueous solution of each of the pollutants, until adsorption-desorption equilibrium. Next, for 3 hours either UV-A illumination by four UV-A Sylvania lamps (350-390 nm, 0.5 mW $cm^{-1}$), or visible illumination by four -Sylvania F15W/54-765- T8 (450-700 nm) lamps was employed. Every 30 minutes the pollutants' characteristic absorption peak was measured with a UV/Vis Hitachi 3010 spectrophotometer equipped with a 60 mm diameter integrating sphere and $BaSO_4$ as a reference. In the case of $Cr^{6+}$, a colorimetric technique with the metal ion indicator diphenylcarbazide (DCP) was applied.

## 3. Results and discussion

### 3.1 XRD and vibrational analysis

As seen in Fig 1a, the characteristic diffraction peaks for pure anatase 25.2°, 36.9°, 37.8°, 38.5°, 48.0°, 53.8°, 55.0°, 62.6°, 68.7° and 70.3°(corresponding to the (101), (103), (004), (112), (200), (105), (211), (204), (116) and (220) Miller indices respectively (Ibrahim, Kaltzoglou, et al., 2020)) as well as the 13° and 27.5° peaks ((001) and (002) planes (Liu et al., 2021)) due to the carbon nitride addition can be observed. The latter reflections appear relatively broad as a result of the small particle size. In Fig. 1b, the expected peaks of pure anatase 145 ($E_g$), 198 ($E_g$), 400 ($B_{1g}$), 515 ($A_{1g}$+$B_{1g}$) and 640 $cm^{-1}$ ($E_g$) (Ibrahim et al., 2019) can be observed at the Raman spectra, while in the composite materials the peaks appear broader. The addition of g-$C_3N_4$, potentially led to a weak 707 $cm^{-1}$ peak, which may be difficult to observe in the composite samples. The final Ag decorated composites present a Raman spectra with the anatase peaks preserved, signifying a substitutional merging of Ag into its structure, with a slight shift for the main anatase peak due to reduced crystallinity and a new low frequency peak (Ibrahim, Kaltzoglou, et al., 2020), thus confirming the presence of $TiO_2$, g-$C_3N_4$ and Ag in the composites without much deviating significantly from the original $TiO_2$ framework.

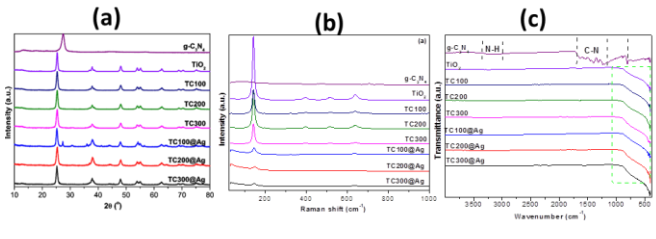


**Figure 1:** XRPD patterns (a); Raman spectra (b); and FT-IR spectra (c) of the composites and their component materials

The FT-IR spectra (Fig. 1c) further confirms the good integration of the source components in the final composites. In the FT-IR spectra of composites the characteristic peaks of g-$C_3N_4$ cannot be observed, potentially due to the good dispersion of the g-$C_3N_4$ layers over $TiO_2$, the loss of long-range order bonding and H-bonding quenching (Safaei et al., 2018).

### 3.2 Photoelectrochemical Characterization

Fig. 2a presents the photocurrent generation analysis on FTO-deposited $TiO_2$/CN/Ag films under UV–VIS illumination. We observe the characteristic transient photocurrents ~~due to the photogenerated hole flux to the film-electrolyte interface~~ and the following decay due to surface recombination.

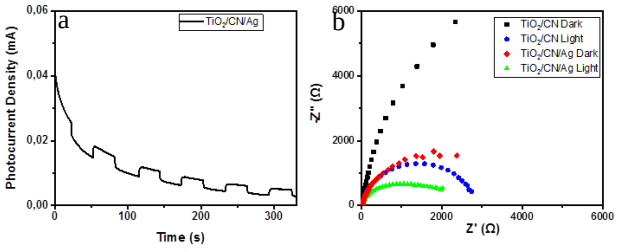


**Figure 2:** UV–VIS irradiation generated transient photocurrent density for $TiO_2$/CN/Ag films (a); Nyquist plots for the composite films under different illumination conditions at Voc (b).

From the EIS analysis on the composite films (with and without silver, Fig. 2b) we can conclude that a lower impedance and charge transfer resistance was the result of the Ag introduction into the $TiO_2$/CN pristine material, leading to impaired recombination in the final samples.

### 3.3 UV DR

From the optical absorption spectra of the materials (UV-Vis, Fig.3a), the slight improvement brought on by the g-$C_3N_4$ integration is overshadowed by the significant enhancement, especially in the Vis region, by the integrated Ag nanoparticle's Surface Plasmon Resonance effect (Ibrahim, Kaltzoglou, et al., 2020), leading to improved light harvesting in a much wider spectral region. The Tauc plots (Fig 3b) reveal a lowered absorption edge for the $TC_X$ samples, followed by an even more significant decrease for the final Ag-composites, explaining their ability to be photoexcited by lower energy light and to perform well in a wide spectrum region.

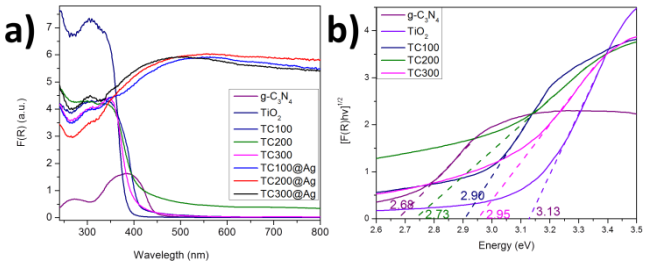


**Figure 3:** Absorption spectra in Kubelka-Munk units (a); Tauc Plots (b) of the composites and their source materials.

### 3.4 Photocatalytic Oxidation of Azo-dyes

The oxidation of RhB and MB by the prepared photocatalysts can be observed at Fig. 4 under both UV and solar illumination. In both cases under UV, the Ag integration provides significant improvements to the pollutant degradation efficiency, especially for our best TC200@Ag sample which reaches 90% (RhB) and 86% (MB) degradation efficiencies after 3 hours. Under solar irradiation, once again, the TC200@Ag surpasses the base-$TiO_2$ material's efficiency. The reduction of $Cr^{6+}$ and PNP by the same photocatalysts can be seen in Fig.5 under UV and solar illumination. Once again, TC200@Ag proves to be the superior photocatalyst under UV while showing significant improvement under solar light as well.

The superiority of the Ag-composite under UV and solar light is caused by the lower band gap but mostly due to the localized surface plasmon resonance effect by the Ag nanoparticles, which allows for photoexited charge carrier migration onto $TiO_2$ (Ibrahim, Kaltzoglou, et al., 2020) and utilization of incident light of even lower energy than UV light. For the oxidation process, scavenger tests show that holes and hydroxyl radicals hold the most significant role, followed by $O_2$, while for the reduction processes $e^-$ seems to hold the key role.

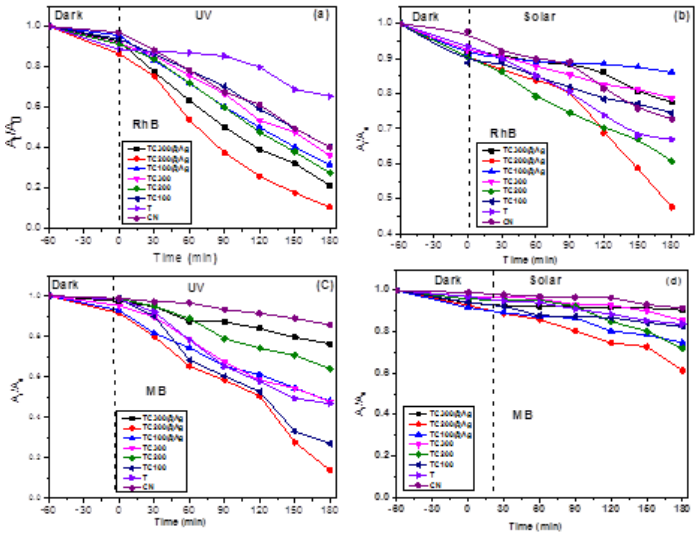


**Figure 4:** Performance of the samples during degradation of RhB under a) UV, and b) solar light, and during degradation of MB under c)UV and D)solar irradiation.

## 4. Conclusion

The integration of carbon nitride and Ag into base-$TiO_2$ has proved to offer significant enhancements to its photo-catalytic performance. Whilst the Ag nanoparticles' SPR effect improves visible light absorption, both g-$C_3N_4$ and Ag suppress recombination. This leads to a superior composite that is able to achieve impressive pollutant degradation efficiencies under both UV and visible light. Furthermore, the $TiO_2/CN_{200}$/Ag nanocomposite exhibits high stability and reusability until the fifth cycle.

## Acknowledgments

The research leading to this work was partially funded by the European Commission, Environment, LIFE17 ENV/GR/000387-PureAgroH2O Programme. P. Falaras acknowledges funding from Prince Sultan Bin Abdulaziz International Prize for Water–Alternative Water Resources Prize 2014.

## References

Alamelu, K., & Ali, B. M. J. (2020). Ag nanoparticle-impregnated sulfonated graphene/$TiO_2$ composite for the photocatalytic removal of organic pollutants. *Applied Surface Science, 512*.

Antoniadou, M., Arfanis, M. K., Ibrahim, I., & Falaras, P. (2019). Bifunctional g-$C_3N_4/WO_3$ Thin Films for Photocatalytic Water Purification. *Water, 11*(12).

Asahi, R., Morikawa, T., Irie, H., & Ohwaki, T. (2014). Nitrogen-Doped Titanium Dioxide as Visible-Light-Sensitive Photocatalyst: Designs, Developments, and Prospects. *Chemical Reviews, 114*(19), 9824-9852.

Chen, Y. X., Liang, Y., Li, T. T., Lin, C. Q., Lin, L., Zhao, M. J., et al. (2019). Hydrothermal fabrication of sandwich-structured Silver sulfide/ferroferric oxide/silver metavanadate graphene microtube using capillary effect for enhancing photocatalytic degradation and disinfection. *Journal of Colloid and Interface Science, 555*, 759-769.

Crake, A., Christoforidis, K. C., Godin, R., Moss, B., Kafizas, A., Zafeiratos, S., et al. (2019). Titanium dioxide/carbon nitride nanosheet nanocomposites for gas phase $CO_2$ photoreduction under UV-visible irradiation. *Applied Catalysis B-Environmental, 242*, 369-378.

Ibrahim, I., Ali, I. O., Salama, T. M., Bahgat, A. A., & Mohamed, M. M. (2016). Synthesis of magnetically recyclable spinel ferrite ($MFe_2O_4$, M = Zn, Co, Mn) nanocrystals engineered by sol gel-hydrothermal technology: High catalytic performances for nitroarenes reduction. *Applied Catalysis B-Environmental, 181*, 389-402.

Ibrahim, I., Athanasekou, C., Manolis, G., Kaltzoglou, A., Nasikas, N. K., Katsaros, F., et al. (2019). Photocatalysis as an advanced reduction process (ARP): The reduction of 4-nitrophenol using titania nanotubes-ferrite nanocomposites. *Journal of Hazardous Materials, 372*, 37-44.

Ibrahim, I., Belessiotis, G. V., Arfanis, M. K., Athanasekou, C., Philippopoulos, A. I., Mitsopoulou, C. A., et al. (2020). Surfactant Effects on the Synthesis of Redox Bifunctional $V_2O_5$ Photocatalysts. *Materials, 13*(20).

Ibrahim, I., Kaltzoglou, A., Athanasekou, C., Katsaros, F., Devlin, E., Kontos, A. G., et al. (2020). Magnetically separable $TiO_2/CoFe_2O_4$/Ag nanocomposites for the photocatalytic reduction of hexavalent chromium pollutant under UV and artificial solar light. *Chemical Engineering Journal, 381*.

Jiang, X. H., Xing, Q. J., Luo, X. B., Li, F., Zou, J. P., Liu, S. S., et al. (2018). Simultaneous photoreduction of Uranium(VI) and photooxidation of Arsenic (III) in aqueous solution over g-$C_3N_4/TiO_2$ heterostructured catalysts under simulated sunlight irradiation. *Applied Catalysis B-Environmental, 228*, 29-38.

Liu, S., Wang, Z., Lu, Y. X., Li, H. P., Chen, X. J., Wei, G. Y., et al. (2021). Sunlight-induced uranium extraction with triazine-based carbon nitride as both photocatalyst and adsorbent. *Applied Catalysis B-Environmental, 282*.

Masih, D., Ma, Y. Y., & Rohani, S. (2017). Graphitic $C_3N_4$ based noble-metal-free photocatalyst systems: A review. *Applied Catalysis B-Environmental, 206*, 556-588.

Park, J. Y., Choi, K. I., Lee, J. H., Hwang, C. H., Choi, D. Y., & Lee, J. W. (2013). Fabrication and characterization of metal-doped $TiO_2$ nanofibers for photocatalytic reactions. *Materials Letters, 97*, 64-66.

Safaei, J., Mohamed, N. A., Noh, M. F. M., Soh, M. F., Riza, M. A., Mustakim, N. S. M., et al. (2018). Facile fabrication of graphitic carbon nitride, (g-$C_3N_4$) thin film. *Journal of Alloys and Compounds, 769*, 130-135.

Wei, W. X., Yu, D., & Huang, Q. L. (2020). Preparation of Ag/$TiO_2$ nanocomposites with controlled crystallization and properties as a multifunctional material for SERS and photocatalytic applications. *Spectrochimica Acta Part a-Molecular and Biomolecular Spectroscopy, 243*.

Ye, T., Chen, W., Xu, H., Geng, N. N., & Cai, Y. (2018). Preparation of $TiO_2$/graphene composite with appropriate N-doping ratio for humic acid removal. *Journal of Materials Science, 53*(1), 613-625.